Road Materials and Pavement Design

ISSN: 1468-0629 (Print) 2164-7402 (Online) Journal homepage: http://www.tandfonline.com/loi/trmp20

Permanent deformation behaviour of a granular material used in low-traffic pavements

Peng Jing, Hossein Nowamooz & Cyrille Chazallon

To cite this article: Peng Jing, Hossein Nowamooz & Cyrille Chazallon (2016): Permanent deformation behaviour of a granular material used in low-traffic pavements, Road Materials and Pavement Design

To link to this article: http://dx.doi.org/10.1080/14680629.2016.1259123

Published online: 08 Dec 2016.

Road Materials and Pavement Design, 2016
http://dx.doi.org/10.1080/14680629.2016.1259123

Taylor & Francis
Taylor & Francis Group

Permanent deformation behaviour of a granular material used in low-traffic pavements

Peng Jing, Hossein Nowamooz and Cyrille Chazallon*

Laboratoire des sciences de l'ingénieur, de l'informatique et de l'imagerie (ICube, UMR 7357, CNRS), INSA de Strasbourg, Strasbourg Cedex, France

(*Received 23 May 2016; accepted 2 November 2016*)

Granular materials are usually used in low-traffic pavement structure as base layer or sub-base layer. The influence of fine content on permanent axial deformation behaviour is significant as well as the water content. This study aims to investigate the permanent axial deformation behaviour of the granular material under cyclic loading at various water contents and various fine contents. A triaxial apparatus is used to obtain permanent axial deformation on the samples prepared with the same dry density at different water contents between 7% and 11% and at different fine contents of 4%, 7.5% and 15.3%. The results show the significant influence of water content and fine content on permanent axial deformation behaviour. The permanent axial deformation increases with the increase of water content while the influence of fine content depends on the water sensitivity of fine particles and their initial water contents. The modified empirical–analytical models are proposed for describing the evolution of permanent axial deformation based on the results in the single-stage test and the multi-stage tests. It takes into account the number of cycles, the stress level, the water content and the fine content of the granular material. Two approaches are used: one based on the water contents and fine contents and the other based on suction values. The approach based on suction values needs less number of parameters to describe permanent axial deformation compared with the approach based on the water contents and fine contents while the two approaches present more or less the same accuracy. The simulation results show a very good capacity of the proposed approaches. These findings reduce the number of tests required to predict permanent axial deformation.

Keywords: granular material; repeated load triaxial tests; permanent deformation; water content; fine content; matric suction

1. Introduction

Low-traffic pavements with a thin bituminous surfacing, granular base and sub-base layers represent approximately 60% of the road network in France. In low-traffic pavements, granular layers play an important role in the overall performance of the structure, especially in permanent deformation behaviour. In these pavements, permanent deformations of the base layer or subgrade represent the main causes of distress that leads to rutting of the pavement surface.

1.1. *Repeated load triaxial test*

Repeated load triaxial test (RLTT) is a common test to investigate the mechanical behaviour of granular materials. It is used to simulate the pavement loading conditions to describe the resilient

*Corresponding author. Email: cyrille.chazallon@insa-strasbourg.fr

behaviour (Bilodeau & Doré, 2012; Caicedo, Coronado, Fleureau, & Correia, 2009; Cary & Zapata, 2011; Duong et al., 2016; Ho, Nowamooz, Chazallon, & Migault, 2014a, 2014b, 2014c; Lekarp, Isacsson, & Dawson, 2000; Nowamooz, Chazallon, Arsenie, Hornych, & Masrouri, 2011; Nowamooz, Ho, Chazallon, & Hornych, 2013; Salour & Erlingsson, 2015a) or permanent axial deformation behaviour (Chazallon, Hornych, & Mouhoubi, 2006; Duong et al., 2013; Gidel, Breysse, Hornych, Chauvin, & Denis, 2001; Hornych, Corte, & Paute, 1993; Puppala, Saride, & Chomtid, 2009; Salour & Erlingsson, 2015b; Trinh et al., 2012; Werkmeister, Dawson, & Wellner, 2004).

In this text, the RLTTs are realised by a pneumatic loading system providing the axial force and confining pressure. Different stress paths ($\Delta q/\Delta p$) can be applied on the sample. The system can measure the axial force directly by a transducer from the head of the sample. During RLTTs, the sample is under the cyclic stress (the confining pressure σ_3 and axial stress σ_1) simulating the pavement solicitation to measure the vertical deformation (ε_1) and the radial deformation (ε_3). For a triaxial test, the mean normal stress p and the shear or deviatoric stress q are defined by

$$p = \frac{\sigma_1 + 2 \cdot \sigma_3}{3}, \tag{1a}$$

$$q = \sigma_1 - \sigma_3, \tag{1b}$$

where σ_1 and σ_3 are the major and minor principal stresses.

In order to stabilise the permanent axial deformation, the samples are subjected to a conditioning phase (or called single-stage test for permanent axial deformation behaviour), which consists of 10,000 cycles applied at a frequency of 0.5 Hz. Ho et al. (2014c) investigated the behaviour of Missillac sand (a well-graded sandy soil) and noted that an equilibrium state was reached after approximately 10,000 load applications. For unbound granular material (UGM), Hornych, Chazallon, Allou, and El Abd (2007) showed that the necessary number of cycles was higher than 50,000.

Besides, due to the limitation of the consuming time and the quantity of materials, it is obviously not realistic to perform repeated triaxial tests on coarse-grained samples to determine the permanent axial deformation at different stress levels. For this reason, multi-stage tests are recommended by Gidel et al. (2001). One sample is subjected to several loading stages with different stress levels for a given stress path. For each loading stage, 10,000 cycles are then applied at a frequency of 0.5 Hz to stabilise the permanent axial deformation.

1.2. *Influence of fine content and water content on mechanical behaviour of granular materials*

Different experimental researches showed that the variation of fine content (particles passing the sieve 75 μm or sieve no. 200 based on American classification) had a significant influence on mechanical behaviour of granular materials as reported by Babić, Prager, and Rukavina (2000), Naeini and Baziar (2004), Kim, Sagong, and Lee (2005), Uthus, Hermansson, Horvli, and Hoff (2006) and Duong et al. (2013).

It has been observed that, if the percentage of fines is not too large (lower than an experimentally defined critical value), the applied stress is supported by the skeleton of coarse grains. On the contrary, when the percentage of fine is high (larger than an experimentally defined critical value), the fine particles take the main role and isolate the coarse grains and consequently modify the soil behaviour (Benahmed, Nguyen, Hicher, & Nicolas, 2015; Chang, Zhang, & Xu, 2012; Dash, Sitharam, & Baudet, 2010).

For the influence of water content, it can be stated that the increase of water content produces an increase of permanent axial deformation, as presented by Gidel, Breysse, and Denis (2002),

Werkmeister, Numrich, Dawson, and Wellner (2003), Uthus et al. (2006), Trinh et al. (2012), Duong et al. (2013) and Salour and Erlingsson (2015b).

Nevertheless, the influence of fine content and water content on permanent deformation behaviour together has been seldom studied.

1.3. *Suction of unsaturated soil*

Unsaturated soils exert an attraction on water, either by capillary action in the pores, between soil particles, or through physicochemical effects. The pressure difference is referred to as matric suction

$$S = u_a - u_w, \tag{2}$$

where u_a is pore air pressure and u_w is pore water pressure. In this paper, matric suction is referred to as suction (S).

The variation of water content with suction is generally represented by a soil water retention curve (SWRC) in unsaturated soil mechanics.

Some researchers have shown that the effect of variation of suction value on the mechanical behaviours of compacted granular materials could be related to the variation of water content (Cary & Zapata, 2011; Han, Mihambanou, & Vanapalli, 2015; Ho et al., 2014a; Kolisoja, Saarenketo, Peltoniemi, & Vuorimies, 2002; Nowamooz et al., 2011; Salour, Erlingsson, & Zapata, 2014; Yang, Lin, Kung, & Huang, 2008).

In some cases (e.g. Ho et al., 2014b; Nowamooz et al., 2011), it could improve the accuracy of evaluating the resilient deformation behaviour based on effective stress concept. Even so, the relationship between permanent axial deformation and suction value has been rarely studied.

1.4. *Models of permanent axial deformation behaviour*

According to the RLTTs, various empirical–analytical models were proposed to predict the permanent axial deformation behaviour taking into account the number of loading cycles (Hornych et al., 1993; Lekarp & Dawson, 1998; Wolff & Visser, 1994), the stress level (Gidel et al., 2001; Korkiala-Tanttu, 2005; Lekarp & Dawson, 1998; Rahman & Erlingsson, 2015) and the water content (Trinh et al., 2012). Besides, based on the shakedown theory, several researchers have developed approaches to calculate either shakedown load or the permanent deformation behaviours (Boulbibane, Collins, Ponter, & Weichert, 2005; Chazallon, Koval, Hornych, Allou, & Mouhoubi, 2009; Sharp & Booker, 1984). However, various empirical models proposed as well as several models using the shakedown approach do not take into account either the effect of water content and fine content together or the influence of suction value.

Among these aforementioned models, Hornych et al. (1993) proposed the following equation which is widely used to simulate the permanent axial deformation with the variation of number of cycles:

$$\varepsilon_1 = A \cdot \left(1 - \left(\frac{N}{N_0}\right)^B\right), \tag{3}$$

where ε_1 is the permanent axial deformation (10^{-4}); N_0 is the number of cycles before the first measurement; N is the number of cycles; A is the final permanent axial deformation (10^{-4}) and B is constant.

Besides, Gidel et al. (2001) modified Hornych's equation to consider additionally the effect of the stress state

$$\varepsilon_1 = \varepsilon_1^{p0} \cdot \left(1 - \left(\frac{N}{N_0}\right)^{-C}\right) \cdot \left(\frac{l_{\max}}{p_a}\right)^{n} \cdot \frac{1}{m + \frac{s}{p_{\max}} - \frac{q_{\max}}{p_{\max}}} = f\,(N) \cdot g(q_{\max}), \tag{4}$$

where $l_{\max} = \sqrt{p_{\max}^2 + q_{\max}^2}$; $p_{\max}$ and $q_{\max}$ are the largest mean stress (kPa) and the largest deviatoric stress (kPa), respectively, for a given stress level, and $(q_{\max} - q_0)/(p_{\max} - p_0) = \Delta q/\Delta p$; p_0 and q_0 are the initial mean stress (kPa) and the initial deviatoric stress (kPa), respectively; ε_1^{p0}, C, n, m, s are constant parameters; $P_a = 100$ kPa.

In this context, the effect of the fine content and the water content on the permanent axial deformation behaviour of Missillac sand is studied with the RLTTs for both single-stage and multi-stage tests. For the analytical modelling, we use principally the framework proposed by Hornych et al. (1993) for the single-stage tests and the framework of Gidel et al. (2001) for the multi-stage tests to estimate the variation of permanent axial deformation of Missillac sand during several loading and unloading cycles. Two approaches will be proposed through these two frameworks: the first based on the water content and fine content and the other based on the suction value.

2. Studied materials

The studied material is the Missillac fine sand. It is an alluvium sand coming from the quarry of Missillac in France. The particle size varies between 0 and 4 mm. This soil is used as subgrade soil in low-traffic pavements for full-scale pavement tests at IFSTTAR (Institut Français des Sciences et Technologies des Transports, de l'Aménagement et des Réseaux) in Nantes, France. The specific gravity G_s of this soil is equal to 2.65. It is sensitive to moisture and its *in situ* elastic modulus typically varies between 50 and 100 MPa.

2.1. *Particle size analysis*

In this study, the natural samples contain three different fine contents:

- M4.0 samples with 4.0% of fine content.
- M7.5 samples with 7.5% of fine content.
- M15.3 samples with 15.3% of fine content (passing through the sieve of 75 μm).

Figure 1 shows the particle size distribution for all of soils (XP P94-041, 1995). Table 1 presents all of the characteristic parameters of these curves, such as C_c and C_u. The coefficients of curvature (C_c) shows a well-graded composition (estimated between 1 and 3) of our studied granular materials.

Table 1 also shows the methylene blue values of M7.5 and M15.3 (NF P94-068, 1993). It states normally that the more the fine content the larger the methylene blue value. Soil can be classified based on the methylene blue values and the particle size distribution (NF P11-300, 1992 or USCS ASTM D2487-06, 2006) as reported in Table 1.

2.2. *Normal proctor tests*

Figure 2 presents the normal proctor compaction curves for M4.0, M7.5 and M15.3. Table 2 shows the optimal water content (OMC) and the maximum dry density (MDD) for the different studied materials.

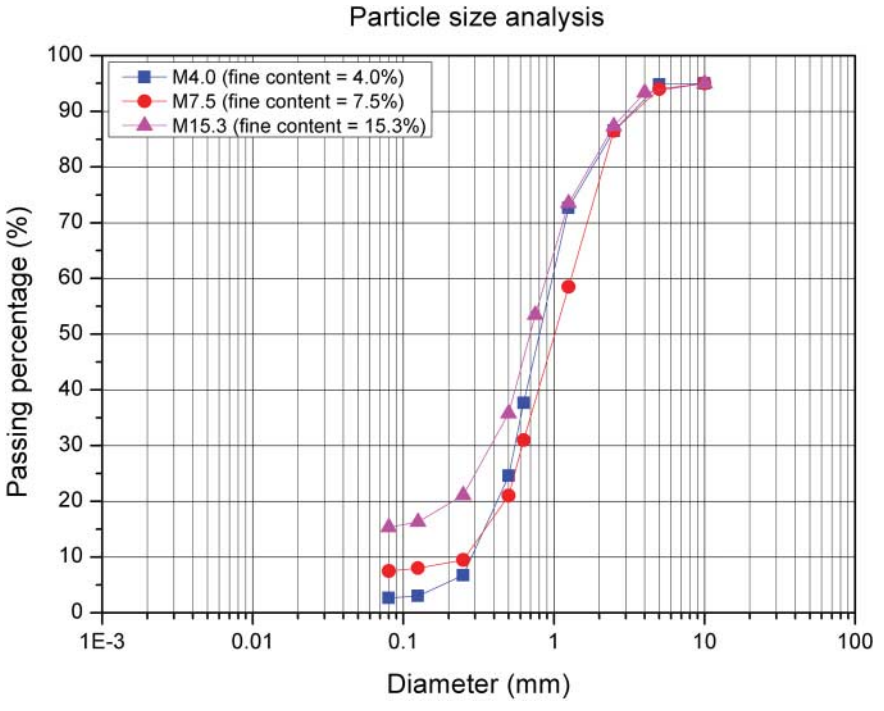

Figure 1. Particle size distribution curves of Missillac sand (M4.0, M7.5 and M15.3).

Table 1. Characteristics of the studied materials.

Materials	Dry density (Mg/m^3)	Fraction (%) 0/80 µm	0.08/0.4 mm	0.4/2 mm	2/4 mm	Particle size d_{60}	d_{30}	d_{10}	C_u	C_c	Blue value	Classification NF	USCS
M4.0	2.00	4	10	76	5	0.95	0.55	0.30	3.17	1.06	–	B2	SP
M7.5	2.00	7.5	6.5	76	5	1.40	0.60	0.25	5.60	1.03	0.56	B2	SP–SC
M15.3	2.00	15.3	14.7	55	10	0.85	0.40	–	8.50	1.88	0.85	B5	SC

Based on the normal proctor compaction curves and the values of OMC and MDD, it can be stated that the OMC and the MDD are almost the same for these three different materials. Consequently, all the samples are prepared in a water content ranging between 7% ($Sr = 57.1\%$) and 11% ($Sr = 89.7\%$) and a dry density close to 2 Mg/m^3 ($e = 0.325$) for the following tests.

2.3. *Soil water retention curve*

The SWRC gives indispensable data to understand the hydraulic behaviour of the unsaturated granular material used in pavement structures. In this study, for the wetting path of the SWRC, the samples are prepared at a water content ranging from 7% ($Sr = 57.1\%$) to 12.3% ($Sr = 100\%$) and for the drying path, the samples initially saturated ($w = 12.3\%$) are dried in the ambient temperature (20°) to reach the desired water content from 7% to 12.3%. The samples are prepared at an initial dry density range of 2 ± 0.06 Mg/m^3.

The matric suction of all the samples, on the wetting and drying paths, is measured by the filter paper technique (ASTM D5298-10, 1995). For matric suction, the soil samples are compacted

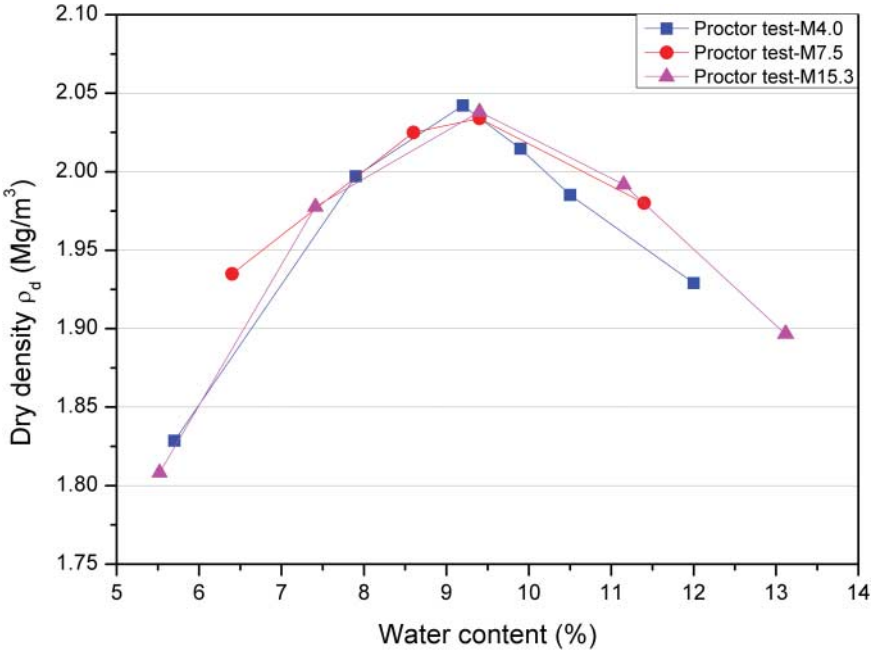

Figure 2. Normal proctor compaction (M4.0, M7.5 and M15.3).

Table 2. Results of normal proctor compaction tests.

Material	OMC (%)	MDD (Mg/m^3)
M4.0	9.3	2.043
M7.5	9.1	2.038
M15.3	9.5	2.040

in two layers with a thickness of 1 and 1.35 cm (M4.0 and M15.3). Whatman No. 42 filter paper is placed between other two pieces of filter papers with a larger diameter. Three filter papers are then inserted between two soil layers. Afterwards, the samples are placed into a sealed jar and maintained for 10 days to reach the state of equilibrium. Finally, the middle piece of filter paper is weighted by a balance with an accuracy of 0.0001 g to obtain the water content of filter paper and then the suction value is determined.

Figure 3 shows the variation of matric suction with water content for both wetting and drying paths for M4.0 and M15.3.

It can be stated that both wetting and drying paths move towards the left side when the fine content decreases. In other words, the higher the fine content the higher the suction value. Similar observations are reported by Caicedo et al. (2009) and Duong, Cui, Tang, Dupla, and Calon (2014).

Based on experimental results, various empirical equations have been suggested to describe the SWRC. Among these equations, the relationships proposed by Brooks and Corey (1964), van Genuchten (1980) and Fredlund and Xing (1994) have been widely used in geotechnical engineering. In this study, we use the van Genuchten model, because of its simplicity and its meaningful parameters. The van Genuchten equation is written as follows:

$$w = w_r + \frac{(w_s - w_r)}{[1 + (\alpha S)^n]^m}, \tag{5}$$

where w is the actual soil water content at the suction S (kPa); w_s (%) and w_r (%) are the saturated water content and the residual water content; α is a parameter related to the air entry suction; m and n are the model parameters with the relationship: $m = 1 - 1/n$.

Figure 4 shows the measured matric suction as well as the model estimations. It presents that the van Genuchten model fits well with the measured values for both studied materials. The parameters are summarised in Table 3.

Figure 4 also shows that the wetting and drying paths join together at a low suction value. We may consider that the wetting and drying paths are unique in this suction range. We define S^* as the suction value corresponding to the intersection point of wetting and drying paths. It is significantly related to fine content. Table 3 summarises the S^* values for different samples.

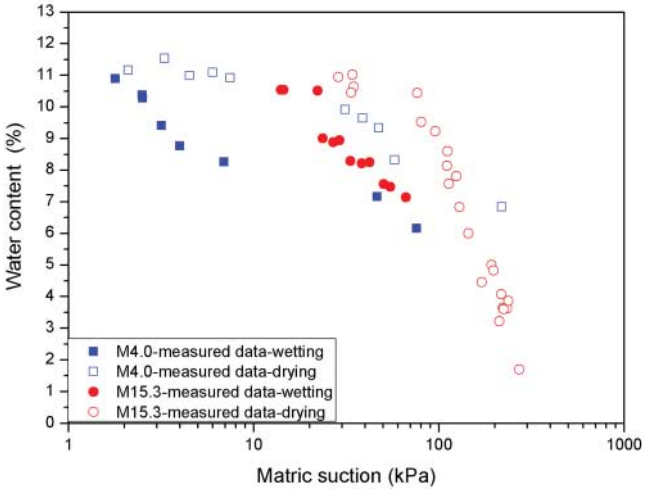

Figure 3. Matric suction obtained by the filter paper method for Missillac sand (M4.0 and M15.3).

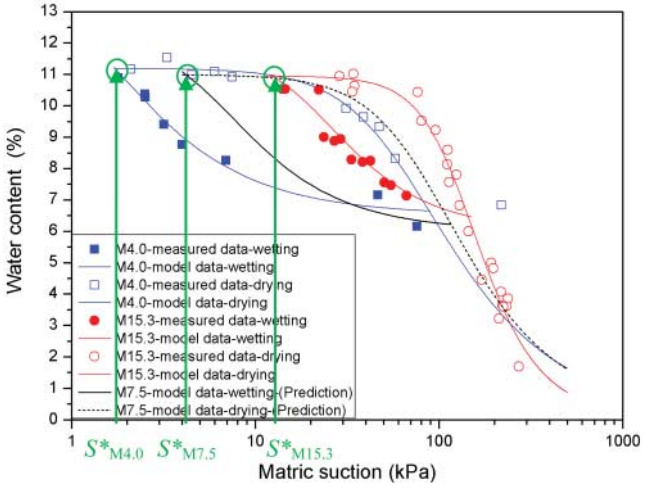

Figure 4. Matric suction obtained by the filter paper method as well as the model prediction (M4.0, M7.5 and M15.3).

Based on the parameters of the van Genuchten model for the samples M4.0 and M15.3, the model parameters and the S^* values are predicted for M7.5 presented in Table 3. Figure 4 also shows the prediction of SWRC for M7.5 both wetting and drying paths.

3. Permanent axial deformation behaviour in a single-stage test

Based on the RLTTs in a single-stage test, the mechanical characteristics of Missillac sand are studied. Afterwards, two approaches are applied to experimental results to predict the permanent axial deformation.

3.1. *Sample preparation and stress paths*

For the experimental procedure, all the samples (M4.0 and M15.3) are compacted following the method of a vibrating hammer (NF EN13286-4, 2003) in seven layers with a height of 285 ± 5 mm and a diameter of 150 mm. Using the vibrating hammer, it can be stated that the compaction time decreases with the increase of the fine content: 45–55 s for M4.0 and 25–35 s for M15.3. All the samples are prepared at a water content range between 7% and 11% with a dry density of 2 ± 0.06 Mg/m^3. For both studied materials, the cyclic stress paths ($\Delta q/\Delta p = 3$) during the conditioning phase are summarised in Table 4.

In this section, we are not able to compare the permanent axial deformation of M7.5 with others (M4.0 and M15.3) because the single-stage tests for this material are performed at a different stress path ($\Delta q/\Delta p = 2$).

3.2. *Experimental result*

The permanent axial deformation increases with the increase of number of cycles at different water contents as illustrated in Figure 5(a) for M4 and in Figure 5(b) for M15.3. The values of $\Delta\varepsilon/\Delta N$ at the end of each test are about 10^{-7} or less than 10^{-7}. For $\Delta\varepsilon/\Delta N$ between 10^{-7} and 10^{-8}, we can state that the permanent axial deformation has achieved the equilibrium state

Table 3. Parameters of the van Genuchten model.

Parameters of VG model	M4.0		M15.3		M7.5 (prediction)	
	Wetting	Drying	Wetting	Drying	Wetting	Drying
α	0.803	0.016	0.049	0.007	0.180	0.012
n	1.929	1.947	2.261	3.025	2.100	2.100
m	0.482	0.486	0.558	0.669	0.524	0.524
w_s (%)	14.3	11.2	11.8	11.0	12.3	11.0
w_r (%)	6.5	0.1	6.0	0.1	6.0	0.1
S^* (kPa)	1.8 ± 0.18		12 ± 1.2		4.2 ± 0.42	

Table 4. Cyclic stress paths in single-stage tests.

Sample	$\Delta q/\Delta p$	Initial stress state (p_0, q_0)	Final (Δp, Δq)	Frequency
M4.0	3	10 kPa, 0 kPa	23.33 kPa, 69.99 kPa	0.5 Hz
M15.3	3	10 kPa, 0 kPa	23.33 kPa, 69.99 kPa	0.5 Hz

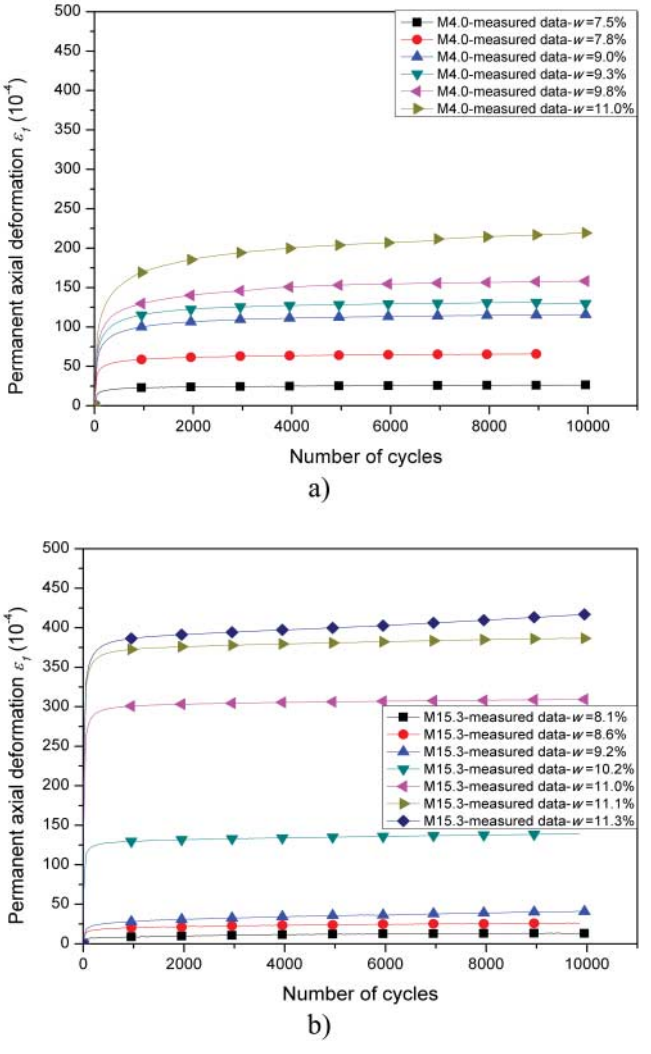

Figure 5. Test results of the single-stage tests: (a) M4.0 and (b) M15.3.

after 10,000 cycles. This value will be later taken as the *A* value of Equation (3) in the analytical approaches of Sections 3.3 and 3.4.

We can observe that the permanent axial deformation increases significantly as the water content increases and the deformation hardly stabilises with the highest water content, such as M4 – 11% (Figure 5(a)) and M15.3 – 11.1% and 11.3% (Figure 5(b)). For the water contents less than 10% for M4 and for the water contents less than 11% for M15.3, the plastic deformation stabilises more quickly when the fine content increases (for M4.0 after 4000 cycles in Figure 5(a) and for M15.3 after 2000 cycles in Figure 5(b)). For the water contents close to the saturation state, more number of cycles is required to reach the stabilised permanent axial deformation.

Figure 6 also shows the variation of the final permanent axial deformation with the water content. It shows that the influence of the fine content is relatively complex: for the water contents between 7% and 10%, the lower the fine content, the higher the permanent axial deformation. Even, the samples M15.3 at a water content less than 8% are very stiff and consequently the

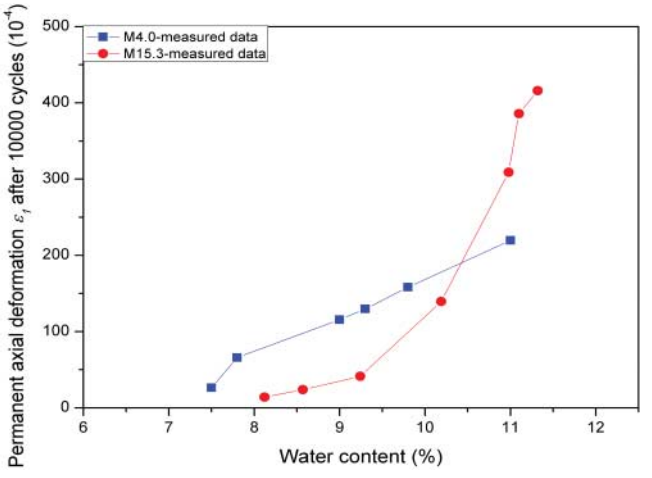

Figure 6. Final permanent axial deformation after 10,000 cycles versus water content (M4.0 and M15.3).

deformations are very small and negligible. For the water content higher than 10.3% (close to the saturated state), the effect of fine content is inversed and the soil with a higher fine content (M15.3) exhibits the higher permanent axial deformation.

These observations can be related to the unsaturated states of samples at different fine contents and water contents. The fine content influences the matric suction significantly as shown above in SWRC (Figures 3 and 4) and the matric suction increases with the increase of the fine content, which makes the soil particles closer. As a result, the unsaturated soil is more resistant to deformation. On the contrary, close to the saturated state, the suction value is almost zero and the fine particles are mainly clay, which decreases the resistance of soil after its combination with water. Similar observations are presented by Seif El Dine, Dupla, Frank, Canou, and Kazan (2010) and Duong et al. (2013). Besides, it is considered that with a content of fine particles below a limit value, the mechanical behaviour is dominated by the skeleton of sand grain and the soil structure could be denser owing to fine particles. Then, when the fine content is higher than this limit value, the mechanical behaviour is governed by fine particles (Benahmed et al., 2015; Chang et al., 2012; Dash et al., 2010).

From SWRC, it is possible to relate the final permanent axial deformation to suction value. Figure 7 shows the final permanent axial deformation versus S (suction) in single-stage tests for samples with two different fine contents. It can be stated that the permanent axial deformation decreases significantly with the increases of suction as explained above. From the results shown in Figure 7, we can observe that the influence of the water content and the fine content cannot be represented by the suction value. With the same suction value, for instance, we can also observe that the higher the fine content, the larger the final permanent axial deformation.

In the last section, we defined a new parameter S^* which is the suction value of the intersection point of wetting and drying paths in SWRC. Figure 8 shows the final permanent axial deformation versus S/S^* for both studied materials. Since the S^* value is very sensitive to any variation of the model parameters, this value is presented in Table 3 in a range of between 90% S^* and 110% S^* for the lower bound and the upper bound of S^*, respectively.

These findings are interesting for the following calculation since only one curve presented in Figure 8 can be used to describe the variation permanent axial deformation with S/S^*. An exponential equation will be proposed for this unique curve in Section 3.4.

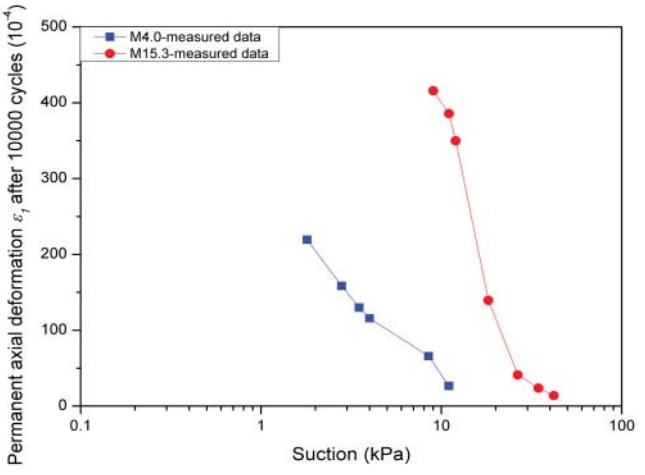

Figure 7. Final permanent axial deformation after 10,000 cycles versus suction (M4.0 and M15.3).

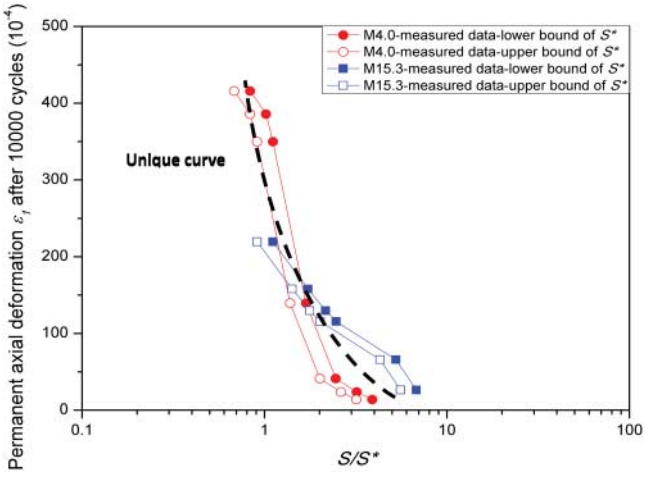

Figure 8. Final permanent axial deformation after 10,000 cycles versus S/S^* (between $S/(110\%\ S^*)$ and $S/(90\%\ S^*)$) (M4.0 and M15.3).

3.3. *Modelling results based on water content and fine content*

Several researchers considered the influence of the water content or the fine content on the mechanical behaviour of granular materials under cyclic loading in their models as shown in Section 1. However, no relationship was proposed to relate the permanent axial deformation to the water content and fine content in literature.

In this section, based on the test results presented in Figure 6, a power function, which represents the "*A*" value in Equation (3), relates the final permanent axial deformation to the water content. The equation can be written as follows:

$$A = a \cdot \left(\frac{w}{k}\right)^{o\cdot(cc)^u}, \tag{6}$$

where A is the final permanent axial deformation (10^{-4}); w is the water content (%); cc is the fine content (%); a, k, o, u are constant.

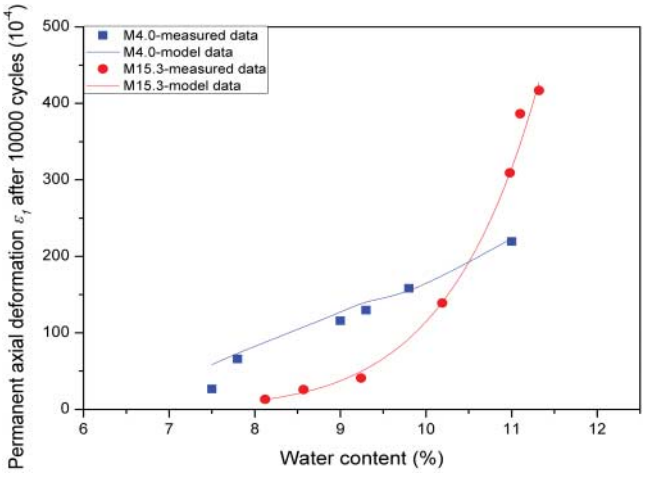

Figure 9. Test results as well as the model prediction for ε_1 after 10,000 cycles versus water content (M4.0 and M15.3).

Figure 9 compares the estimated A value with the measured axial deformation after 10,000 cycles versus water content. It can be stated that this model fits the experimental results well.

Another required parameter in Equation (3) is the power B. The parameter B controls the shape of evolution of permanent axial deformation with number of cycles. The variation curve of permanent axial deformation becomes flatter when B (absolute value) increases. The test results presented in Figure 5 show that the higher the water content, the smaller the B value, and the higher the fine content, the larger the B value. Based on these results, we propose the following equation for B:

$$B = \left(\frac{k'}{w}\right) + o' \cdot cc, \tag{7}$$

where k' and o' are constant.

Combining Equations (6) and (7), the modified Equation (3) can be written as follows:

$$\varepsilon_1 = a \cdot \left(\frac{w}{k}\right)^{o\cdot(cc)^u} \cdot \left(1 - \left(\frac{N}{N_0}\right)^{\left(\frac{k'}{w}\right)+o'\cdot cc}\right). \tag{8}$$

Figure 10 shows the comparison between the proposed model for ε_1 (Equation (8)) and the experimental results. Generally, it can be stated that the proposed model fits very well qualitatively and quantitatively with most the experimental results. The parameters of the proposed model are summarised in Table 5. Table 5 also shows that only one set of parameters required to take into account the number of cycles, the water content and the fine content with a good global correlation coefficient.

Based on the simulation results in Figure 10, the proposed model can describe correctly the permanent axial deformation of Missillac sand. However, six parameters are necessary to be calibrated in these calculations if the water content and the fine content are considered in the proposed approach. Therefore, in the next section the fine content and water content will be replaced by suction to reduce the number of parameters affecting the mechanical soil behaviour.

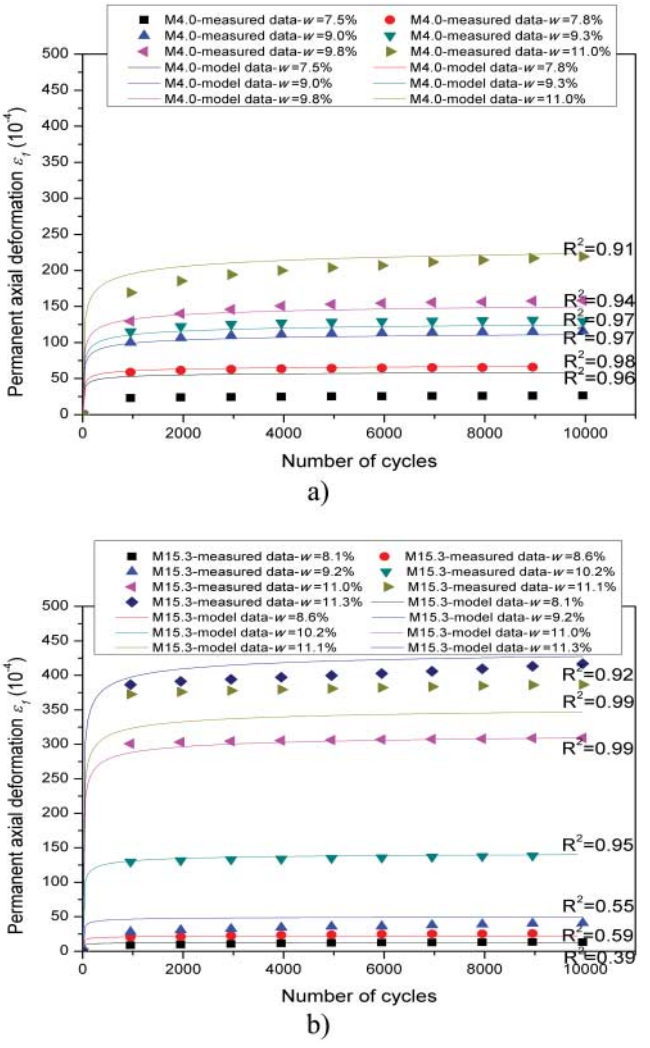

Figure 10. Test results as well as the model prediction for ε_1 based on water content and fine content: (a) M4.0 and (b) M15.3.

3.4. *Modelling results based on suction value*

In view of the pervious results presented in Figure 8, a simple power function relationship is proposed between final permanent axial deformation A and S/S^* value

$$A = b \cdot \left(\frac{S}{S^*}\right)^d, \tag{9}$$

where S is the suction value (kPa); b and d are constant.

Figure 11 compares the measured and predicted permanent axial deformation after 10,000 cycles versus S/S^*. It can be stated that Equation (9) can predict correctly the final permanent axial deformation.

As shown in Figure 10, Equation (8) describes the B value (the curve shape) well. In order to relate the B value with suction value, Figure 12 shows the calculated B values by Equation (8)

Table 5. Parameters of the model for the single-stage tests based on water content and fine content.

Missillac sand	a	k	o	R^2
	238.058	10.661	1.264	
	u	k'	o'	0.94
	0.782	− 1.800	− 0.012	

versus variations of the suction value for M4.0 and M15.3. It can be observed that there is a linear relationship between the B value and the ln(S/Sa) value (Sa is equal to 100 kPa).

Based on Figure 12, we propose the following equation for B:

$$B = e \cdot \ln\left(\frac{S}{S_a}\right) + f\,, \tag{10}$$

where S_a is equal to 100 kPa; e and f are constant.

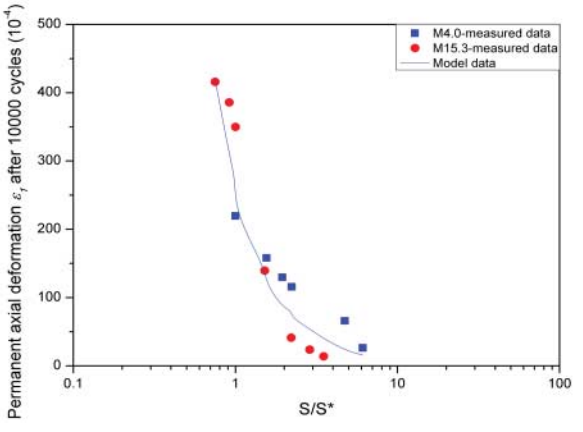

Figure 11. Test results as well as the model prediction for ε_1 after 10,000 cycles versus S/S* (M4.0 and M15.3).

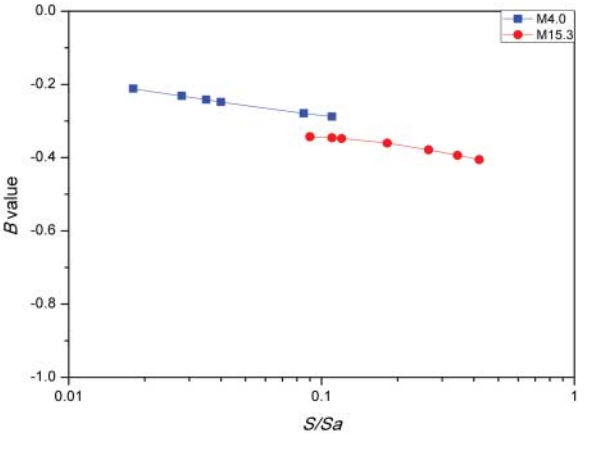

Figure 12. Calculated B values by Equation (8) versus S/S_a (M4.0 and M15.3).

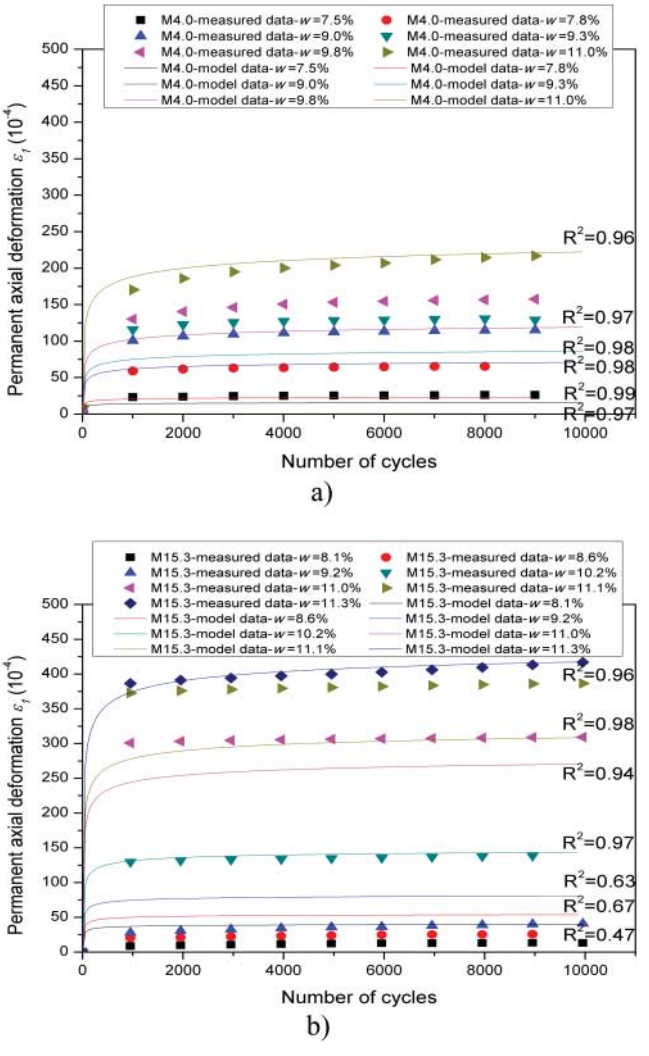

Figure 13. Test results as well as the model prediction for ε_1 based on suction value: (a) M4.0 and (b) M15.3.

As a result, a modified Equation (3) can be written as follows:

$$\varepsilon_1 = b \cdot \left(\frac{S}{S^*}\right)^d \cdot \left(1 - \left(\frac{N}{N_0}\right)^{e \cdot \ln(S/S_a)+f}\right). \tag{11}$$

Figure 13 shows the comparison between the proposed model for ε_1 (Equation (11)) and the experimental results. For M4.0, the model values are close to the measured value at the lowest water content (7.5%) and the highest water content (11%). The model values are lower than the measured values for the other four water contents, which shows the obvious difference between model values and measured values. For M15.3, the model value is close to the measured value at the water content of 10.2% and the highest water content of 11.3%. The model values are higher than the measured values at water contents lower than 10.2% and are lower than measured values

Table 6. Parameters of the model for the single-stage tests based on suction value.

Missillac sand	b	d	R^2
	300.000	− 1.569	
	e	f	0.90
	− 0.060	− 0.400	

at water contents higher than 10.2%. Generally, it can be stated that the proposed model fits right with the experimental results. The parameters of the proposed model are summarised in Table 6.

3.5. *Discussion*

Generally, it can be observed that there is an optimum fine content, which corresponds to the minimum permanent axial deformation at a given water content. It is difficult to estimate this optimum fine content because it changes drastically with the variation of water content.

For the water contents less than 10.3% (or maybe the optimum proctor water content), the increase of fine content reduces the permanent axial deformation. In other words, the optimum fine content corresponds to the highest studied fine content.

On the other hand, for the water content higher that 10.3%, the decrease of fine content reduces the permanent axial deformation (Figure 6). In other words, the optimum fine content reaches its minimum value at a water content close to the saturated state. However we need more experiments particularly at one or two other fine contents to determine accurately the minimum optimum fine content at the saturated state of our studied materials. This point will be further investigated in our future studies.

To solve the problem of dual variation of the permanent axial deformation with the water content and the fine content and to avoid the determination of the optimum fine content, the permanent axial deformation is related to suction values. A unique curve may define the variation of the permanent axial deformation with S/S^* value. These findings are helpful for an easier interpretation of the results. Besides, it can be stated that the model based on the suction value has less parameters (b, d, e, f) than the model based on the water content and fine content which has two more parameters (a, k, o, u, k', o').

4. Permanent axial deformation behaviour in a multi-stage test

The same as the single-stage tests in Section 3, the previous two approaches are applied to model the results of RLTT in a multi-stage test.

4.1. *Sample preparation and stress paths*

For sample preparation, the samples M15.3 are compacted following the method of a vibrating hammer (NF EN13286-4, 2003) in seven layers with a height of 285 ± 5 and a diameter 150 mm, the same as the single-stage tests. The samples M7.5 are compacted following the method of Vibrocompaction (NF P98-230-1, 1992) in one layer with a height of 320 ± 5 mm and a diameter of 160 mm. Based on the study of Balay, Correia, Jouve, Hornych, and Paute (1998) on unbound granular material, it can be stated that the dry density with the vibrating hammer method in seven layers is approximately same with the vibrocompaction method.

During the test procedure, one sample at a given water content is subjected to a series of loading stages with different deviatoric stresses on a given stress path and each loading stage

includes 10,000 cycles. The water content and the stress state applied to M7.5 and M15.3 are shown in Tables 7 and 8, respectively.

For M7.5, the different stress paths ($\Delta q/\Delta p = 3$, $\Delta q/\Delta p = 2$, $\Delta q/\Delta p = 1.5$ and $\Delta q/\Delta p = 1$) are applied to different samples with constant water content (11%) from an initial stress state of $(p_0, q_0) = (10, 5$ kPa) at the frequency of 1 Hz. For M15.3, the different samples are prepared with different water contents ($w = 7.7\%$, $w = 9.4\%$, $w = 9.9\%$ and $w = 11.1\%$), and then a constant stress path ($\Delta q/\Delta p = 3$) is applied to the samples from an initial stress state of $(p_0, q_0) = (10, 0$ kPa) at the frequency of 0.5 Hz.

4.2. *Experimental result*

Figure 14(a,b) presents the permanent axial deformation versus the number of cycles at the different stress levels in multi-stage tests for M7.5 and M15.3, respectively. It implies that the evolution of the permanent axial deformation is also related to the stress state: the higher the stress path or the higher the stress level, the larger the permanent axial deformation. The influence of the water content is the same as the single-stage tests: the higher the water content, the larger the permanent axial deformation.

Besides, comparing the results of M7.5 with M15.3 for stress path $\Delta q/\Delta p = 3$, stress levels $\Delta q = 40$ kPa and $\Delta q = 70$ kPa and a water content $w = 11\%$, it can be also observed that the sample close to the saturated state with a higher fine content exhibits less mechanical resistance as it has been shown in the single-stage test.

Table 7. Cyclic stress paths in the multi-stage tests for M7.5.

w (%)	11.0		11.0		11.0		11.0	
Sr(%)	89.79		89.7		89.7		89.7	
Stress path	Initial stress state $(p_0, q_0) = (10, 5$ kPa); frequency $f = 1$ Hz							
	$\Delta q/\Delta p = 3$		$\Delta q/\Delta p = 2$		$\Delta q/\Delta p = 1.5$		$\Delta q/\Delta p = 1$	
	Δq (kPa)	Δp (kPa)	Δq (kPa)	Δp (kPa)	Δq (kPa)	Δp (kPa)	Δq (kPa)	Δp (kPa)
Level 1	40	13.3	40	20	40	26.6	40	40
Level 2	60	20	60	30	60	40	60	60
Level 3	70	23.3	80	40	80	53.3	80	80
Level 4	–	–	100	50	100	66.6	120	120
Level 5	–	–	120	60	120	80	–	–
Level 6	–	–	140	70	140	93.3	–	–

Table 8. Cyclic stress paths in the multi-stage tests for M15.3.

w (%)	7.7		9.4		9.9		11.1	
Sr(%)	62.8		76.6		80.7		90.5	
Stress path	Initial stress state $(p_0, q_0) = (10, 0$ kPa); frequency $f = 0.5$ Hz							
	$\Delta q/\Delta p = 3$		$\Delta q/\Delta p = 3$		$\Delta q/\Delta p = 3$		$\Delta q/\Delta p = 3$	
	Δq (kPa)	Δp (kPa)	Δq (kPa)	Δp (kPa)	Δq (kPa)	Δp (kPa)	Δq (kPa)	Δp (kPa)
Level 1	40	13.3	40	13.3	40	13.3	40	13.3
Level 2	70	23.3	70	23.3	70	23.3	70	23.3
Level 3	100	33.3	100	33.3	100	33.3	–	–
Level 4	140	46.7	140	46.7	140	46.7	–	–

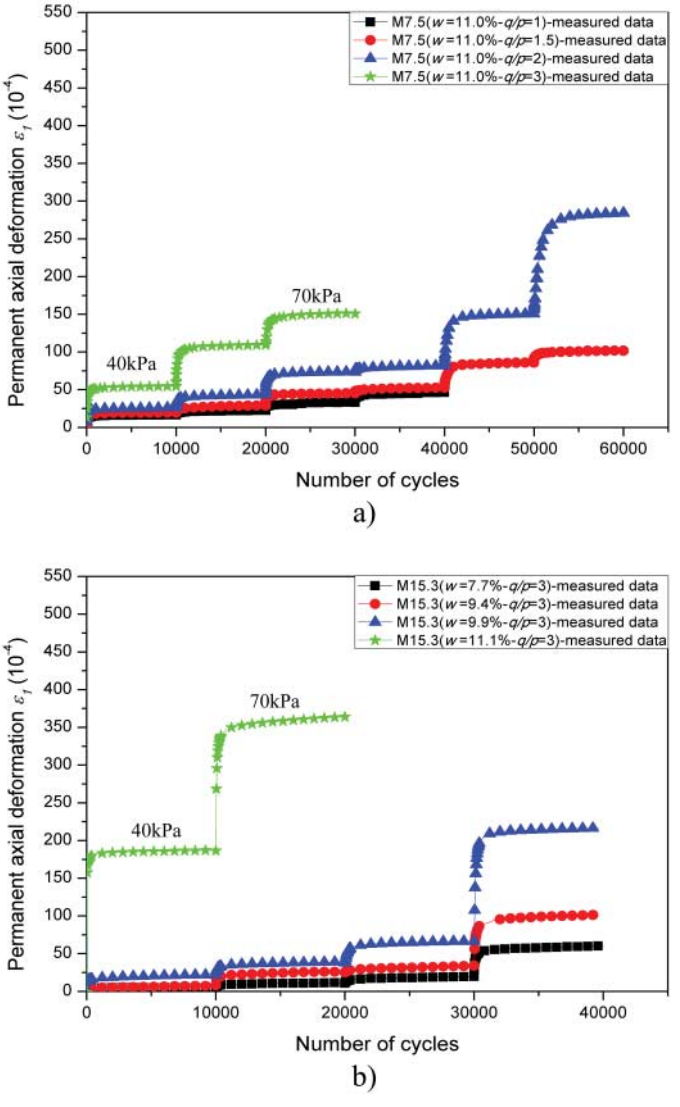

Figure 14. Test results of the multi-stage tests: (a) M7.5 and (b) M15.3.

4.3. *Modelling results based on water content and fine content*

Based on Equations (4) and (8), a new equation is proposed for estimating multi-stage RLTTs as follows:

$$\varepsilon_1 = R \cdot \left(1 - \left(\frac{N}{N_0}\right)^{((k'/w)+o' \cdot cc)}\right) \cdot \left(a \cdot \left(\frac{w}{k}\right)^{o \cdot (cc)^u}\right) \cdot \left(\frac{l_{\max}}{p_a}\right)^n \cdot \frac{1}{m + \frac{s}{p_{\max}} - \frac{q_{\max}}{p_{\max}}}, \qquad (12a)$$

where w is the water content (%); cc is the fine content (%); $l_{\max} = \sqrt{p_{\max}^2 + q_{\max}^2}$; $p_{\max}$ (kPa) and $q_{\max}$ (kPa) are the largest mean stress and the largest deviatoric stress, respectively, per load cycle; $P_a = 100$ kPa; R, a, k, o, u, k', o', m, s and n are constants.

In this context, all multi-stage test results are used to determine the model parameters by following the next two steps:

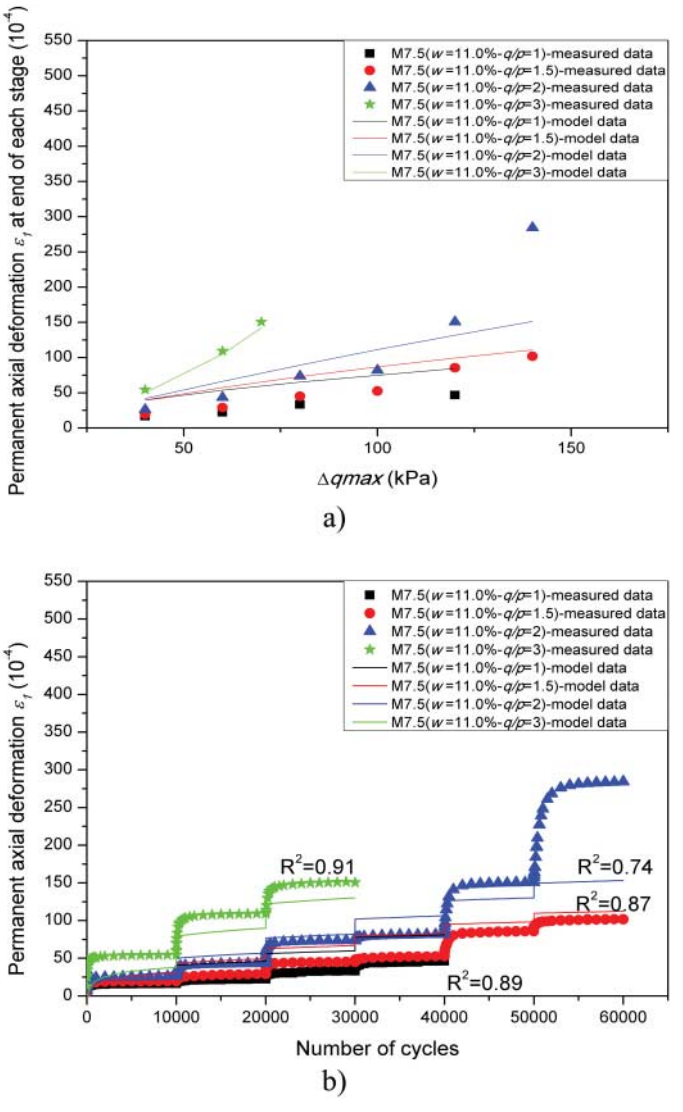

Figure 15. Test results as well as the model prediction for ε_1 based on water content and fine content for M7.5. (a) Cumulated permanent axial deformation at the end of each loading stage. (b) Variation of the permanent axial deformation with the number of cycles.

Step 1: Determine parameters a, k, o, u, m, s and n by fitting $g(q_{\max}, cc, w)$ in Equation (12b) for the cumulated permanent axial deformation obtained at the end of each loading stage as shown in Figure 15(a) and Figure 16(a)

$$g(q_{\max},\ cc, w) = \left(a \cdot \left(\frac{w}{k}\right)^{o\cdot(cc)^u}\right) \cdot \left(\frac{l_{\max}}{p_a}\right)^n \cdot \frac{1}{m + \frac{s}{p_{\max}} - \frac{q_{\max}}{p_{\max}}}. \tag{12b}$$

Equation (12a) could be rewritten as

$$\varepsilon_1 = R \cdot \left(1 - \left(\frac{N}{N_0}\right)^{((k'/w)+o'\cdot cc)}\right) \cdot g(q_{\max},\ cc, w). \tag{12c}$$

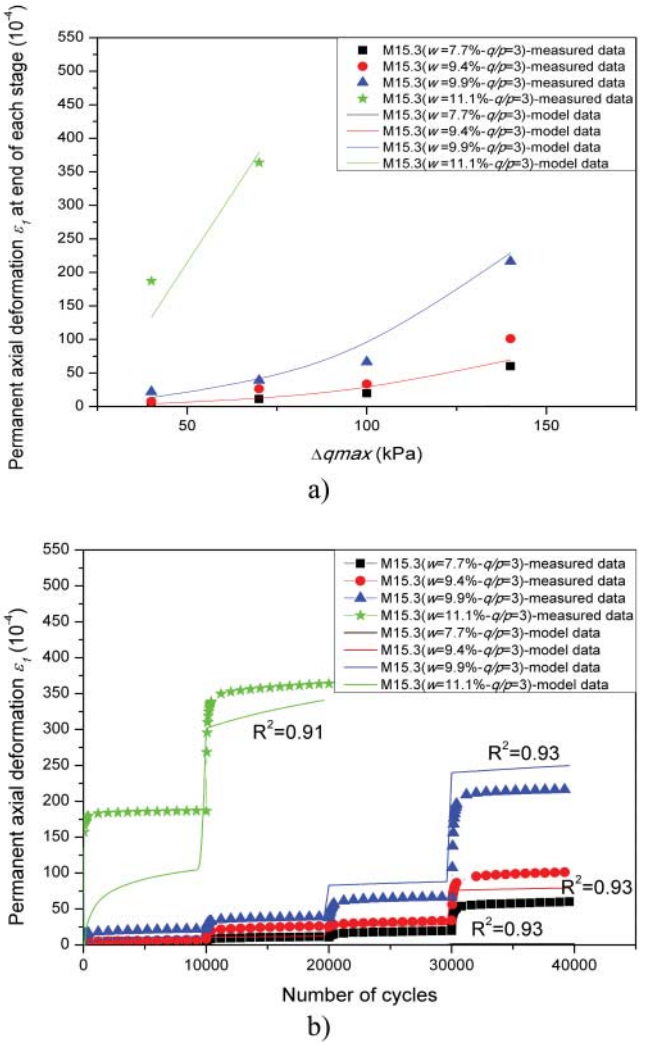

Figure 16. Test results as well as the model prediction for ε_1 based on water content and fine content for M15.3.

Table 9. Parameters of the model for the multi-stage tests based on water content and fine content.

Missillac sand	a	k	o	u	m	R^2
	51.111	10.140	1.377	1.003	2.620	
	s	n	R	k'	o'	0.74
	25.693	0.500	4.235	− 0.443	− 0.0003	

Step 2: Determine parameters R, k', o' by fitting Equation (12c) to the permanent axial deformation evolution with the number of cycles, as shown in Figures 15(b) and 16(b).

All these parameters were summarised in Table 9 and the simulation results are presented in Figures 15(b) and 16(b). However, the accuracy is less than the single-stage test because of the different stress paths and the different stress levels to be taken into account in the calibration, the results show a good capacity of the model to estimate the permanent axial deformation behaviour for Missillac sand.

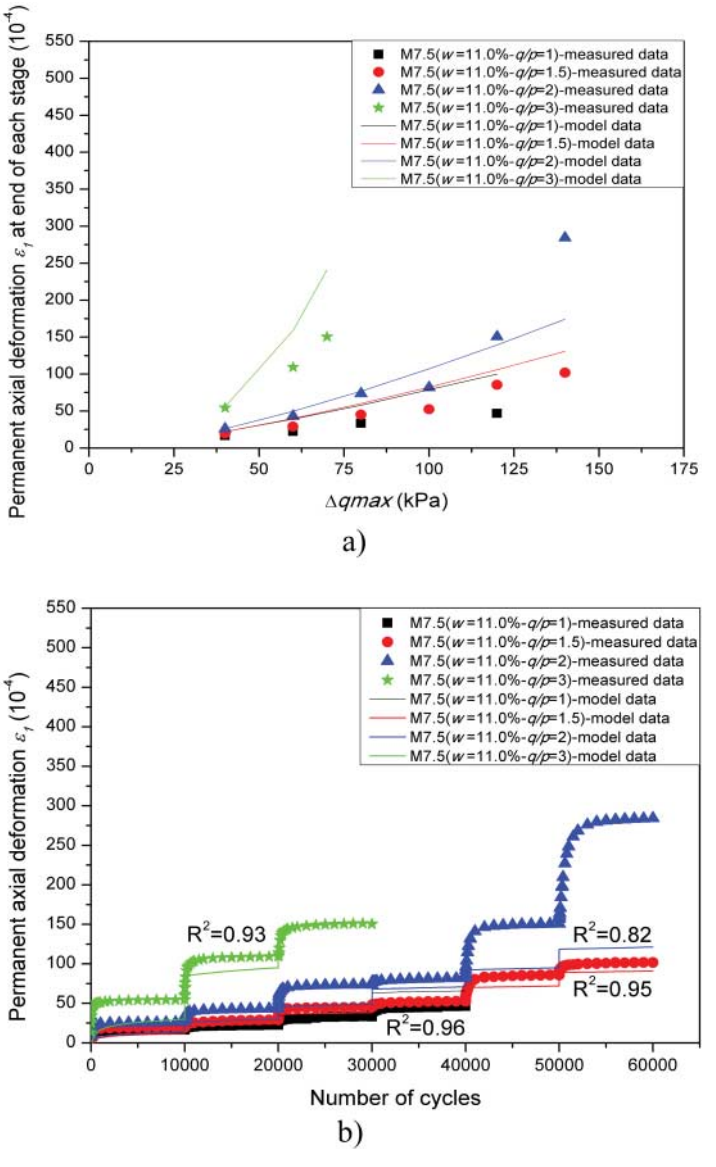

Figure 17. Test results as well as the model prediction for ε_1 based on suction value for M7.5.

4.4. *Modelling results based on suction value*

The permanent axial deformation in the multi-stage tests can be also related to suction value. Based on Equations (4) and (11), a new equation, which considers the different stress states, is also proposed to estimate the permanent axial deformation behaviour, as follows:

$$\varepsilon_1 = T \cdot \left(1 - \left(\frac{N}{N_0}\right)^{e\cdot\ln(S/Sa)+f}\right) \cdot b \cdot (S/S^*)^d \cdot \left(\frac{l_{\max}}{p_a}\right)^n \cdot \frac{1}{m + \frac{s}{p_{\max}} - \frac{q_{\max}}{p_{\max}}}, \tag{13a}$$

where S is the suction value (kPa); S^* is the suction value (kPa) of the intersection point of wetting and drying paths in SWRC; Sa is equal to 100 kPa; $l_{\max} = \sqrt{p_{\max}^2 + q_{\max}^2}$; $p_{\max}$ (kPa)

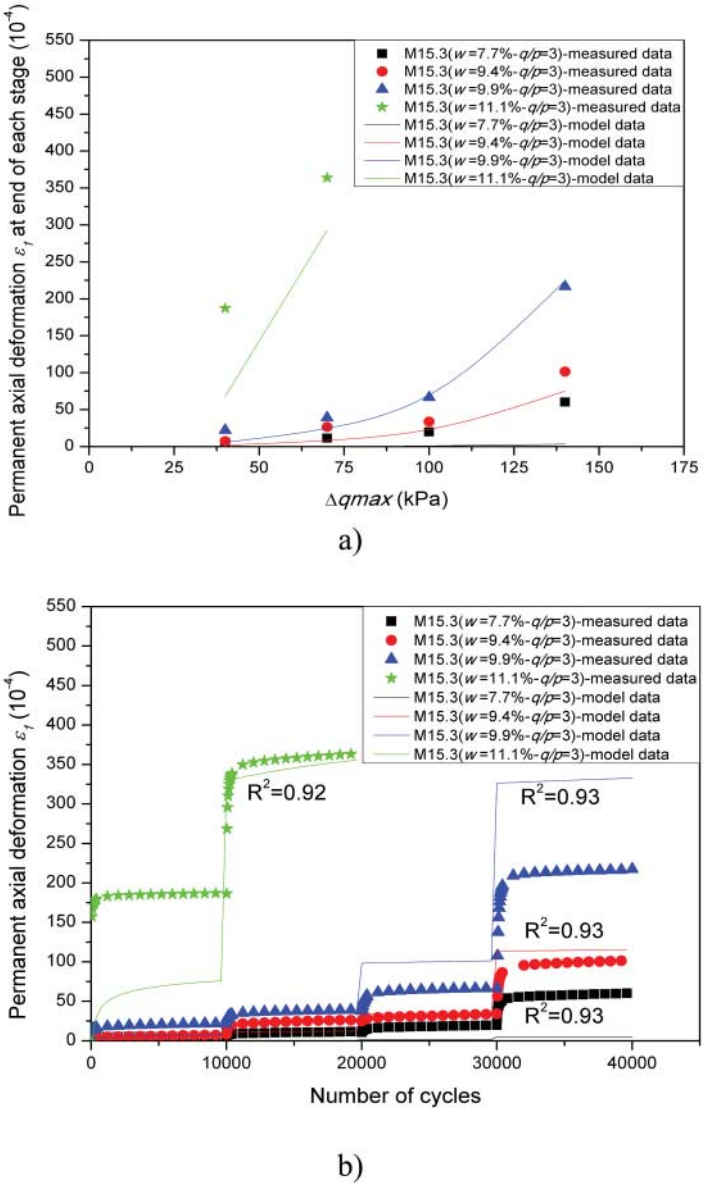

Figure 18. Test results as well as the model prediction for ε_1 based on suction value for M15.3.

and $q_{\max}$ (kPa) are the largest mean stress and the largest deviatoric stress, respectively, per load cycle; $P_a = 100$ kPa. T, b, d, e, f, m, s, and n are constant.

The same procedure is used to determine the model parameters:

Step 1: Determine parameters b, d, m, s and n by fitting $g(q_{\max}, S)$ in Equation (13b) for the cumulated permanent axial deformation obtained at the end of each loading stage as shown in Figures 17(a) and 18(a).

$$g(q_{\max},\ S) = b \cdot (S/S^*)^d \cdot \left(\frac{I_{\max}}{p_a}\right)^n \cdot \frac{1}{m + \frac{s}{p_{\max}} - \frac{q_{\max}}{p_{\max}}}. \tag{13b}$$

Table 10. Parameters of the model for the multi-stage tests based on suction value.

Missillac sand	b	d	m	s	R^2
	98.421	− 4.547	2.873	9.392	
	n	T	e	f	0.67
	1.291	1.812	− 0.134	− 0.499	

Equation (13a) could be rewritten as

$$\varepsilon_1 = T \cdot \left(1 - \left(\frac{N}{N_0}\right)^{e \cdot \ln(S/Sa)+f}\right) \cdot g(q_{\max}, S). \tag{13c}$$

Step 2: Determine parameters T, e, f by fitting Equation (13c) to the permanent axial deformation evolution with the number of cycles as shown in Figures 17(b) and 18(b).

All these parameters were summarised in Table 10. Figures 17 and 18 show the test results and the modelling results. Generally, it suggests that the simulation is in good agreement with the experimental results. Moreover, the accuracy is not far from the model based on the fine content and the water content.

4.5. *Discussion*

As it was mentioned for the single-stage tests, the comparison of these two series of modelling results shows that the model (Equation (12a)) based on water content and fine content is moderately more accurate ($R^2 = 0.74$) than the model (Equation (13a)) based on suction value ($R^2 = 0.67$). However, the number of parameters of the proposed model is obviously decreased when it is based on suction value: Equation (13a) with 8 parameters (T, b, d, e, f, m, s and n) compares to Equation (12a) with 10 parameters (R, a, k, o, u, k', o', m, s and n).

5. Conclusions

This paper investigates the permanent axial deformation of the Missillac sand in low-traffic pavements under cyclic loading at various initial moisture states. A series of RLTTs are applied on the different remolded soil samples at different water contents and different fine contents in a single-stage procedure. Another series of tests are carried out at different fine contents, different water contents and different stress states in a multi-stage procedure. Both in single-stage tests and multi-stage tests, the results show that the permanent axial deformation increases with the increase of the water content, while the influence of fine content depends on the initial water content and the water sensitivity of fine particles. Increasing the stress path and the stress level leads to an increase of the permanent axial deformation in a multi-stage test.

To describe the permanent axial deformation of Missillac sand, based on the Hornych model (Equation (3)) and Gidel model (Equation (4)), this paper proposes a new empirical–analytical model taking into account the effect of the water content, the fine content, the number of cycles and the stress state. The simulation results show a good capacity of this proposed model to evaluate the permanent axial deformation in both single-stage tests and multi-stage tests.

Besides, the SWRCs are obtained by the filter paper method for Missillac sand at different fine contents. To solve the problem of dual variation of the permanent axial deformation with the water content and the fine content and to avoid the determination of the optimum fine content (which is complicated in this study), the permanent axial deformation is related to suction values.

A unique curve may define the variation of the permanent axial deformation with S/S^* value. These findings are helpful for an easier interpretation of the results. Besides, it can be stated that the model based on the suction value has less parameters than the model based on the water content and fine content which has two more parameters.

These two proposed models could reduce the number of tests required to predict the soil permanent axial deformation.

For the pavement structures, this study is also useful to understand the permanent deformation behaviour of the granular materials, especially for the sandy material. The tendency should be the same with other clayey sand without particle breakage. For silty material, we think that the influence on hydraulic mechanical behaviour caused by fine particles and suction will be strengthened, whereas the trend of gravelly material will be opposite, with a low suction range. Meanwhile, the particle breakage could be induced during the cyclic loading for a gravelly material with a high stress level. In the future, this study will be expanded for non-standard UGM (including higher fine content, higher plasticity index, higher methylene blue value and more crushable grains).

Indeed, under the successive loading and unloading cycles and the environmental solicitations, particles damage may accidentally occur which leads to fine content changes. At the same time, the unsaturated granular soil is influenced significantly by water content changes (rainfall, drainage or evaporation). As it was previously observed, the fine particles are very sensitive to water content changes and to avoid the controversial effect of the water sensitivity, the determination of the optimum fine content (especially close to the saturated state) may be helpful for the pavement design. This work as well as further numerical modelling will be conducted in future studies.

Acknowledgements

The previous work of Pierre Hornych (IFSTTAR) and Xuan Nam Ho (INSA-Strasbourg) is acknowledged.

Disclosure statement

No potential conflict of interest was reported by the authors.

Funding

This work is supported by the China Scholarship Council [grand number 201304490044].

References

ASTM D2487-06. (2006). *Standard practice for classification of soils for engineering purposes (unified soil classification system)*.

ASTM D5298-10. (1995). *Standard test method for measurement of soil potential (suction) using filter paper*.

Babić, B., Prager, A., & Rukavina, T. (2000). Effect of fine particles on some characteristics of granular base courses. *Materials and Structures*, *33*(7), 419–424.

Balay, J., Correia, A. G., Jouve, P., Hornych, P., & Paute, J. L. (1998). Etude expérimentale et modélisation du comportement mécanique des graves non traitées et des sols supports de chaussées. *Dernières Avancées, Bulletin Des Laboratoires Des Ponts Et Chaussees*, *216*, 3–18.

Benahmed, N., Nguyen, T. K., Hicher, P. Y., & Nicolas, M. (2015). An experimental investigation into the effects of low plastic fines content on the behavior of sand/silt mixtures. *European Journal of Environmental and Civil Engineering*, *19*(1), 109–128.

Bilodeau, J. P., & Doré, G. (2012). Water sensitivity of resilient modulus of compacted unbound granular materials used as pavement base. *International Journal of Pavement Engineering*, *13*(5), 459–471.

Boulbibane, M., Collins, I. F., Ponter, A. R. S., & Weichert, D. (2005). Shakedown of unbound pavements. *Road Materials and Pavement Design*, *6*(1), 81–96.
Brooks, R. H., & Corey, A. T. (1964). *Hydraulic properties of porous media*. Hydrology paper, no. 3. Fort Colins: The Department of Civil Engineering, Colorado State University.
Caicedo, B., Coronado, O., Fleureau, J. M., & Correia, A. G. (2009). Resilient behavior of non standard unbound granular materials. *Road Materials and Pavement Design*, *10*(2), 287–312.
Cary, C. E., & Zapata, C. E. (2011). Resilient modulus for unsaturated unbound materials. *Road Materials and Pavement Design*, *12*(3), 615–638.
Chang, D. S., Zhang, L. M., & Xu, T. H. (2012). Laboratory investigation of initiation and development of internal erosion in soils under complex stress states. *Proceedings of the 6th conference on Scour and Erosion* (pp. 895–902), Paris.
Chazallon, C., Hornych, P., & Mouhoubi, S. (2006). Elastoplastic model for the long-term behavior modeling of unbound granular materials in flexible pavements. *International Journal of Geomechanics*, *6*(4), 279–289.
Chazallon, C., Koval, G., Hornych, P., Allou, F., & Mouhoubi, S. (2009). Modelling of rutting of two flexible pavements with the shakedown theory and the finite element method. *Computers and Geotechnics*, *36*(5), 798–809.
Dash, H. K., Sitharam, T. G., & Baudet, B. A. (2010). Influence of non plastic fines on the response of a silty sand to cyclic loading. *Soils and Foundations*, *50*, 695–704.
Duong, T. V., Cui, Y. J., Tang, A. M., Dupla, J. C., & Calon, N. (2014). Effect of fine particles on the hydraulic behavior of interlayer soil in railway substructure. *Canadian Geotechnical Journal*, *51*(7), 735–746.
Duong, T. V., Cui, Y. J., Tang, A. M., Dupla, J. C., Canou, J., Calon, N., & Robinet, A. (2016). Effects of water and fines contents on the resilient modulus of the interlayer soil of railway substructure. *Acta Geotechnica*, *11*(1), 51–59.
Duong, T. V., Tang, A. M., Cui, Y. J., Trinh, V. N., Dupla, J. C., Calon, N., . . . Robinet A. (2013). Effects of fines and water contents on the mechanical behavior of interlayer soil in ancient railway sub-structure. *Soils and Foundations*, *53*(6), 868–878.
Fredlund, D. G., & Xing, A. (1994). Equations for the soil–water characteristic curve. *Canadian Geotechnical Journal*, *31*(4), 521–532.
van Genuchten, M. T. (1980). A closed-form equation for predicting the hydraulic conductivity of unsaturated soils. *Soil Science Society of America Journal*, *44*(5), 892–898.
Gidel, G., Breysse, D., & Denis, A. (2002). Influence de l'état hydrique et des sollicitations routières sur l'évolution du comportement des graves non traitées calcaires utilisées en assise de chaussée. *Revue Française De Génie Civil*, *6*(5), 789–799.
Gidel, G., Breysse, D., Hornych, P., Chauvin, J. J., & Denis, A. (2001). A new approach for investigating the permanent deformation behavior of unbound granular material using the repeated load triaxial apparatus. *Bulletin Des Laboratoires Des Ponts Et Chaussees*, *233*, 5–21.
Han, Z., Mihambanou, B., & Vanapalli, S. K. (2015). A new approach for estimating the influence of soil suction on the resilient modulus of pavement subgrade soils. *Airfield and Highway Pavements*, *2015*, 861–872. doi:10.1061/9780784479216.076
Ho, X. N., Nowamooz, H., Chazallon, C., & Migault, B. (2014a). Effect of hydraulic hysteresis on low-traffic pavement deflection. *Road Materials and Pavement Design*, *15*(3), 642–658.
Ho, X. N., Nowamooz, H., Chazallon, C., & Migault, B. (2014b). Effective stress concept for the effect of hydraulic hysteresis on the resilient behavior of low traffic pavements. *International Journal of Pavement Engineering*, *16*(9), 842–856.
Ho, X. N., Nowamooz, H., Chazallon, C., & Migault, B. (2014c). Influence of fine content and water content on the resilient behavior of a natural compacted sand. *Road Materials and Pavement Design*, *15*(3), 606–621.
Hornych, P., Chazallon, C., Allou, F., & El Abd, A. (2007). Prediction of permanent deformations of unbound granular materials in low traffic pavements. *Road Materials and Pavement Design*, *8*(4), 643–666.
Hornych, P., Corte, J. F., & Paute, J. L. (1993). Etude des déformations permanentes sous chargements répétésde trois graves non traitées. *Bulletin Des Laboratoires Des Ponts Et Chaussees*, *184*, 45–55.
Kim, D., Sagong, M., & Lee, Y. (2005). Effects of fine aggregate content on the mechanical properties of the compacted decomposed granitic soils. *Construction and Building Materials*, *19*(3), 189–196.

Kolisoja, P., Saarenketo, T., Peltoniemi, H., & Vuorimies, N. (2002). Laboratory testing of suction and deformation properties of base course aggregates. *Transportation Research Record: Journal of the Transportation Research Board*, *1787*, 83–89.

Korkiala-Tanttu, L. (2005). A new material model for permanent deformations in pavements. *Proceedings of the 7th conference on bearing capacity of roads and airfields* (pp. V1–V12), Trondheim.

Lekarp, F., & Dawson, A. (1998). Modelling permanent deformation behavior of unbound granular materials. *Construction and Building Materials*, *12*(1), 9–18.

Lekarp, F., Isacsson, U., & Dawson, A. (2000). State of the art. I: Resilient response of unbound aggregates. *Journal of Transportation Engineering*, *126*(1), 66–75.

Naeini, S. A., & Baziar, M. H. (2004). Effect of fines content on steady-state strength of mixed and layered samples of a sand. *Soil Dynamics and Earthquake Engineering*, *24*(3), 181–187.

NF EN13286-4. (2003). *Mélanges traités et mélanges non traités aux liants hydrauliques. Méthodes l'essai pour la masse volumique de référence et la teneur en eau en laboratoire-Marteau vibrant*.

NF P11-300. (1992). *Exécution des terrassements-Classification des matériaux utilisables dans la construction des remblais et des couches de forme d'infrastructures routières*.

NF P94-068. (1993). *Sols: reconnaissance et essais-Mesure de la quantité et de l'activité de la fraction argileuse-Détermination de la valeur de bleu de méthylène d'un sol par l'essai à la tache*.

NF P98-230-1. (1992). *Préparation des matériaux traités aux liants hydrauliques ou non traités. Fabrication des éprouvettes par vibrocompression*, 8 p.

Nowamooz, H., Chazallon, C., Arsenie, M. I., Hornych, P., & Masrouri, F. (2011). Unsaturated resilient behavior of a natural compacted sand. *Computers and Geotechnics*, *38*(4), 491–503.

Nowamooz, H., Ho, X. N., Chazallon, C., & Hornych, P. (2013). The effective stress concept in the cyclic mechanical behavior of a natural compacted sand. *Engineering Geology*, *152*(1), 67–76.

Puppala, A. J., Saride, S., & Chomtid, S. (2009). Experimental and modeling studies of permanent strains of subgrade soils. *Journal of Geotechnical and Geoenvironmental Engineering*, *135*(10), 1379–1389.

Rahman, M. S., & Erlingsson, S. (2015). Predicting permanent deformation behavior of unbound granular materials. *International Journal of Pavement Engineering*, *16*(7), 587–601.

Salour, F., & Erlingsson, S. (2015a). Resilient modulus modelling of unsaturated subgrade soils: Laboratory investigation of silty sand subgrade. *Road Materials and Pavement Design*, *16*(3), 553–568.

Salour, F., & Erlingsson, S. (2015b). Permanent deformation characteristics of silty sand subgrades from multistage RLT tests. *International Journal of Pavement Engineering*. doi:10.1080/10298436.2015.1065991

Salour, F., Erlingsson, S., & Zapata, C. E. (2014). Modelling resilient modulus seasonal variation of silty sand subgrade soils with matric suction control. *Canadian Geotechnical Journal*, *51*(12), 1413–1422.

Seif El Dine, S., Dupla, J., Frank, R., Canou, J., & Kazan, Y. (2010). Mechanical characterization of matric coarse-grained soils with a large-sized triaxial device. *Canadian Geotechnical Journal*, *47*(4), 425–438.

Sharp, R. W., & Booker, J. R. (1984). Shakedown of pavements under moving surface loads. *Journal of Transportation Engineering*, *110*(1), 1–14.

Trinh, V. N., Tang, A. M., Cui, Y. J., Dupla, J. C., Canou, J., Calon, N., … Schoen O. (2012). Mechanical characterisation of the fouled ballast in ancient railway track substructure by large-scale triaxial tests. *Soils and Foundations*, *52*(3), 511–523.

Uthus, L., Hermansson, Å., Horvli, I., & Hoff, I. (2006). A study on the influence of water and fines on the deformation properties and frost heave of unbound aggregates. *Cold Regions Engineering*, 1–13. doi:10.1061/40836(210)65.

Werkmeister, S., Dawson, A. R., & Wellner, F. (2004). Pavement design model for unbound granular materials. *Journal of Transportation Engineering*, *130*(5), 665–674.

Werkmeister, S., Numrich, R., Dawson, A., & Wellner, F. (2003). Design of granular pavement layers considering climatic conditions. *Transportation Research Record: Journal of the Transportation Research Board*, *1837*, 61–70.

Wolff, H., & Visser, A. T. (1994). Incorporating elasto-plasticity in granular layer pavement design. *Proceedings of the Institution of Civil Engineers: Transport*, *105*(4), 259–272.

XP P94-041. (1995). *Sols: reconnaissance et essais-Identification granulométrique-Méthode de tamisage par voie humide*.

Yang, S. R., Lin, H. D., Kung, J. H. S., & Huang, W. H. (2008). Suction-controlled laboratory test on resilient modulus of unsaturated compacted subgrade soils. *Journal of Geotechnical and Geoenvironmental Engineering*, *134*(9), 1375–1384.